The thermally activated deformation behaviour of single-crystalline microcast aluminium wires

Journal Article

Author(s):
Verheyden, Suzanne; Deillon, Léa; Mortensen, Andreas

Publication date:
2022-08-01

Permanent link:
https://doi.org/10.3929/ethz-b-000550012

Originally published in:
Acta Materialia 234, https://doi.org/10.1016/j.actamat.2022.118037

Acta Materialia 234 (2022) 118037

Contents lists available at ScienceDirect

Acta Materialia

journal homepage: www.elsevier.com/locate/actamat

The thermally activated deformation behaviour of single-crystalline microcast aluminium wires

S. Verheyden [a], L. Deillon [a,b], A. Mortensen [a,*]

[a] Mechanical Metallurgy Laboratory, École Polytechnique Fédérale de Lausanne, MXD 140 (Bâtiment MXD), Station 12, Lausanne CH-1015, Switzerland
[b] Advanced Manufacturing Lab, ETH Zürich, Technoparkstr. 1, Zürich CH-8005, Switzerland

ARTICLE INFO

Article history:
Received 24 December 2021
Revised 13 May 2022
Accepted 14 May 2022
Available online 16 May 2022

Keywords:
Plasticity size effect
Thermal activation
Microcasting
Aluminium
Intermittent plasticity

ABSTRACT

A microcasting process is used to produce high aspect ratio (>30) monocrystalline pure aluminium wires with a diameter between 14 and 115 µm. The role of thermal activation in the plastic deformation of these microwires is measured by means of (single) tensile stress relaxation tests. The microwires deform largely in an intermittent fashion, *i.e.*, through repeated sudden displacement bursts, also during stress relaxation, implying that the bursts can be triggered through thermal activation. By separating the intermittent and the continuous parts of the stress relaxation load *vs*. time signal, we measure an activation area characteristic of the continuous relaxation mechanism. Haasen plots of the continuous relaxation data suggest the presence of a back-stress on the order of 2.5 MPa, which can be attributed to the thin layer of oxide covering the metal. Smaller (14–25 µm) diameter crystals oriented for single slip show highly scattered activation area values and a steeper rate of increase of data in the Haasen plot than all other samples, which conform, save for the back-stress, with what is observed in bulk aluminium. Present findings are consistent with data from commensurate aluminium crystals in replicated microcellular structures. Data of this work show that, in single slip within aluminium crystals, the coupling between the activation area and the flow stress is altered when crystals are below 30 µm in diameter. The absence of a systematic difference in data between samples produced of 4N or 5N aluminium suggests that this conclusion is characteristic of the pure metal.

1. Introduction

The plastic deformation behaviour of small (≤ 100 µm) dislocation-containing monocrystalline metallic crystals has been the focus of extensive research over the past two decades; reviews can be found in [1–5]. In such small crystals, both the initial dislocation density and the size of the crystal define the progression of plastic deformation [4,6]. With a sufficient number of initial dislocations present (as opposed to a dislocation-starved state found in sub-micron diameter samples), the deformation of small crystals is often governed by the action of single arm sources, the length of which scales with dimensions of the crystal [7–9].

Most small-scale plasticity studies probe focused ion beam (FIB) milled micro- and nanopillars [2,3,10–12], a method that is known to create a specific surface state, comprising notably ion-implantation, in the samples that it produces [13–19]. FIB-free alternatives for the production of monocrystalline micro-samples include the selective etching of eutectic alloys [20,21], patterned electrodeposition [22–26], silicon lithography [18] and an embossing technique [27,28]. Microcasting, a casting process designed to produce micrometric samples, is another approach for the production of microscopic samples free of surface ion implantation. The process has previously been shown to produce net-shape, dislocation-containing, 99.99% pure monocrystalline aluminium microwires of diameter (D) between 7 and 120 µm. When loaded in tension, the microwires demonstrate characteristics of the plasticity size effect: their yield strength scales as D^{-1} (as expected for single-arm dislocation sources) and becomes increasingly stochastic with decreasing D [9]. Plastic deformation in thinner cast microwires progresses largely through sudden displacement bursts, visible as quasi-instantaneous load drops, of highly variable amplitude, the cumulative distribution function (CDF) of which follows a power law distribution at smaller amplitudes, followed by an exponential distribution at larger amplitudes [9,29,30].

Some explorations of the plasticity size effect address thermally activated deformation, be it by means of creep, strain-rate jump or stress relaxation tests, to find generally that as the sampled volume decreases, the strain-rate sensitivity increases and the activa-

* Corresponding author.
E-mail address: andreas.mortensen@epfl.ch (A. Mortensen).

https://doi.org/10.1016/j.actamat.2022.118037

tion volume decreases [5,23,24,26,31–45]. The thermally activated deformation of micron-scale aluminium was characterized by Xiao et al. [34] using strain-rate jump tests, to find activation volumes on the order of 100 b^3 (where b is the burgers vector length) and a significant influence on data of FIB-induced ion implantation. Ng and Ngan [31] studied the creep deformation of Al micropillars and showed that intermittency is also observed during a creep hold. It is also relevant to cite the work by Diologent et al. [46] who performed stress relaxation tests on open-pore microcellular aluminium, which is a material consisting of many monocrystalline micro-struts of diameter that can be made smaller than 100 µm. Their data show that below a certain strut size (on the order of a few tens of micrometre), one observes in both pure Al and Al-5wt%Mg a halving of the slope in a plot of the inverse of the (dimensionless) apparent activation area versus the stress at which stress relaxation is initiated, a frequently used and highly informative plot known as a Haasen plot [47–49].

The literature on the thermally activated plastic deformation of bulk (meaning of diameter on the order of, or exceeding, one millimetre) face-centred cubic single-crystals is far more extensive. Many of those studies were published in the 1950's and 1960's, and were often triggered by the seminal work of Cottrell and Stokes [50]. Basinski and Basinski summarized the most important findings from this period in Ref. [51]. The Cottrell-Stokes relation was observed to hold in Stage II of single crystal deformation, a deviation therefrom being observed both in Stage I and Stage III. The onset of Stage III deformation is typically associated with an upward deviation from linearity in the Haasen plot [52–54]. The literature is mixed on the origin and the direction of the deviation from the Cottrell-Stokes relation in Stage I: sometimes data on a Haasen plot display a higher slope than in Stage II, while in other cases a lower slope is reported [55–62]. Those deviations have at times been attributed to impurities, which tended to be more frequent in samples of earlier work [41,61].

Given this known influence of the single crystal deformation stage on the thermal activation of plastic flow, and knowing also that microcrystals deform far more in Stage I of single FCC crystal deformation than do their bulk counterparts [63–66], one is entitled to expect a significant influence of sample dimensions on the thermally activated plastic flow of microcrystals. Building on this observation, we aim here to contribute to our understanding of the size effect in thermally activated plasticity using microcast aluminium microwires that are tested for stress relaxation in uniaxial tensile deformation. Unlike most work to date on thermally actived plastic flow in small-scale samples, we use here relaxation tests, known to give more precise insight in thermally activated plastic deformation than do alternative test methods [67,68]. Other distinguishing features of this work are that we explore systematically, in terms of the resolved stress and by means of relaxation tests conducted on tensile samples unaffected by FIB machining, the influence of crystal orientation on microsample plasticity, and the correlation between the thermal activation of continuous plastic flow and the sample flow stress.

2. Experimental procedures

2.1. Microwire preparation and characterization

Aluminium (99.99 and 99.999%) microwires are prepared through the microcasting process that is described in Krebs et al. [9]. In a nutshell, the process consists in pressure infiltrating monocrystalline salt (NaCl) moulds containing cavities that have the shape of the castings to be produced. The salt moulds are produced through slow evaporation of brine baths (Sigma Aldrich NaCl ≥99.8 purity in water, 200 g/l) containing a nylon precursor. Following the random growth and retrieval of each salt single crystal that will be used to produce a mould, the polymer precursor onto which it grew is removed by pyrolysis (600 °C, 4.5 h). Several salt moulds of this kind are then simultaneously pressure-infiltrated with molten Al (T∼700 °C) using argon gas (15 bar) followed by directional solidification. The final aluminium castings are then freed through dissolution of each infiltrated salt mould in a water-based chromate solution (0.84 g/l $NaHCO_3$ and 1.62 g/l Na_2CrO_4), thus releasing the thin aluminium wires in a gentle, non-invasive manner that minimizes oxidation of their surface. Each microwire is then glued (Loctite 496^{TM}) to a holder specifically made for stable placement in a custom-built tensile testing apparatus.

The crystallographic orientation of the microwires is random; it is therefore measured for each microwire. This was done using single-crystal X-ray diffraction (Enraf Nonius FR590, by Dr. Kurt Schenk). Scanning electron microscopy (SEM, Zeiss Merlin) images are systematically taken prior to testing to verify the surface quality of the microwires, to measure their diameter, and to verify its uniformity along the gauge length. Following tensile testing, which was in all tests reported here performed up to failure, SEM images are again taken, now with focus on observation of the slip steps that have formed along the wire surface during deformation.

2.2. Tensile tests

All tensile and relaxation tests are performed using the custom-built displacement-controlled tensile machine and procedure that are described in Refs. [9,30]. Three different datasets are acquired during a typical test: (i) time-displacement-force data acquired at 50 Hz, (ii) time-force data acquired at 50 kHz and (iii) optical images of the gauge length, acquired at 2 Hz. All tensile plots are based on the 50 Hz data, as are the apparent activation area (a) calculations (see Section 2.5). The plastic deformation of the microwires being intermittent, the high-frequency 50 kHz data are used to capture the nearly instantaneous load drops.

A 10 g or 50 g Futek (Irvine, USA) LPM200 load cell is used for microwires of diameter D below or above 50 µm respectively. For all tests a displacement rate of 300 nm/s is imposed, corresponding (given that samples are ≈ 1 mm long) to strain rates on the order of $3{\cdot}10^{-4}$ s^{-1}. To lower the noise level of the load signal, the 50 kHz time-force data are filtered four times by means of a moving average filter over 250 points (this approximates a Gaussian filter [69]).

Knowing the orientation of the crystal making each tensile sample, stress-strain curves are then converted following standard procedures [64] to curves of resolved shear stress versus resolved shear strain. Given the many interruptions caused by sudden displacement events and by relaxation cycles, the (average) work hardening rate of the crystals is computed using only stress values from the upper envelope of the tensile test curves. The slope of that curve, or in other words the tensile work hardening rate of the microwire, is found to often evolve with deformation from a relatively constant low value to higher values, reminiscent of the transition from Stage I to Stage II of FCC single crystal deformation. We identify the location of this transition using the inflexion point in the plot of (this upper envelope of) stress versus strain.

2.3. Stress relaxation tests

In a stress relaxation test, the sample is loaded up to a predefined stress or strain level at which point the cross-head of the machine is stopped and the (decreasing) stress is recorded versus time [67,70]. In this work, individual 60 s long stress relaxations are triggered at predefined load levels. The number of stress relaxations performed on a given microwire therefore depends (among other parameters) on the amount of work hardening during the test. The stability of the set-up was initially checked using stiffer

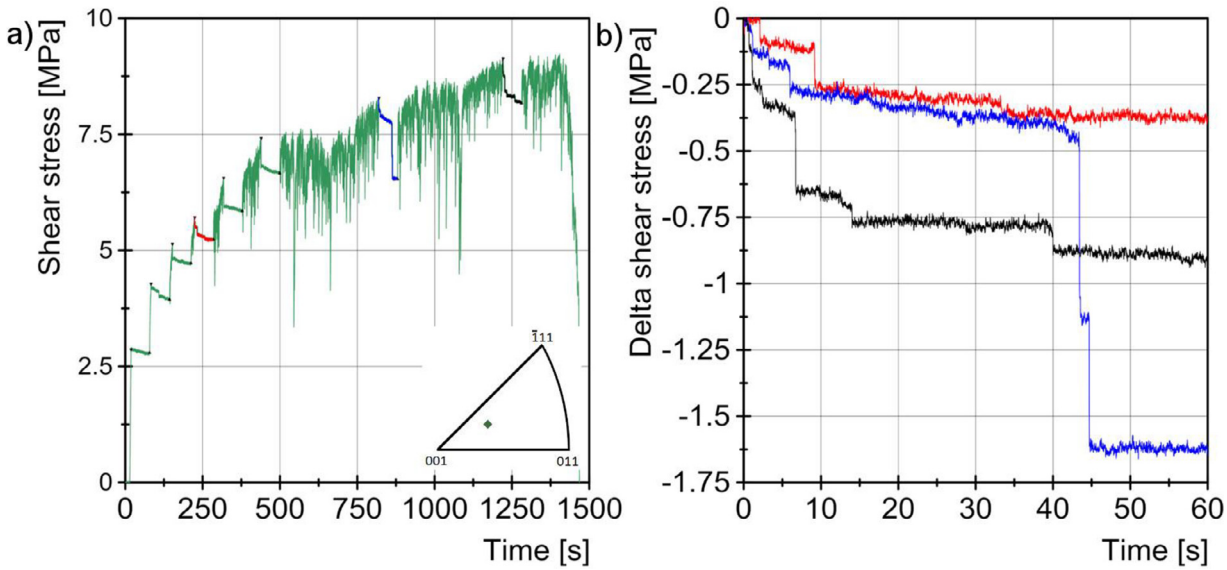

Fig. 1. (a) Curve of resolved shear stress curve *versus* time, containing multiple (single) stress relaxations (60 s) at different stress levels for a Al4N microwire oriented for single slip (D = 14.7 µm). (b) Extract of a selection of the performed relaxations: during stress relaxation, displacement jumps occur along the wire.

dummy samples, which showed that the tensile bench is sufficiently stiff and free of time-dependent deformation mechanisms for relaxation testing to generate meaningful data.

The imposed stress relaxations contain sudden displacement events. Those are of somewhat lower frequency than while the sample is strained forcibly, yet are still clearly present, Fig. 1: on average 2–3 events are detected per 60 s-long stress relaxation. The fact that stress relaxations contain sudden load drops complicates data treatment, because those drops change the shape of normally smooth, continuous stress-relaxation plots into a sloping staircase-shaped line, Fig. 1. To extract from those data a meaningful activation area, a method was developed, based on the following assumptions:

(i) That continuous relaxation processes within the loaded microwires give a signal that follows the frequently observed law, in which the stress decrement ($\Delta\tau$) varies logarithmically with time (t) [67,71]:

$$\Delta\tau = -\frac{kT}{ba}\ln\left(\frac{t}{c}+1\right) \tag{1}$$

where a is the activation area defined as:

$$a = \frac{kT}{b}\frac{\partial \ln\left(-\frac{\dot{\tau}}{M}\right)}{\partial\tau} \tag{2}$$

with τ the resolved shear stress measured from the moment the load train is stopped during a uniaxial test on a (plastically flowing) sample, M the load train rigidity, k the Boltzmann constant, T the temperature in Kelvin (293 K here), and b the Burgers vector (=0.286 nm for Al);

(ii) and that a sudden displacement event does not alter the state of the material differently than would continuous relaxation after the same stress decrease. This latter assumption is justified by the fact that the activation area calculated from (continuous) stress relaxation data carries information on the motion of dislocations moving at numerous locations along the entire microwire length, whereas sudden load drops are caused by one or a few highly localized dislocation sources. Dislocations not in close proximity to the active single arm source(s) will therefore sense only the resulting decrease in stress.

Operationally, the method involves three main steps: (1) binning $\Delta\tau$ data to smoothen their time derivative, (2) identifying and discarding bins that correspond to sudden displacement jumps and (3) calculating the apparent activation area based on the remaining data bins, taking into account the progressive error on the datapoints. Once the data are collected, the apparent activation volume is derived from a linear regression through data points that have been tagged as relevant. A full description of the method is given in Ref. [30], which also gives access to full datasets for all samples of this work (listed in Table 1 of Ref. [30]).

3. Results

Monocrystalline aluminium microwires of 99.99% purity (4N) were produced to have a diameter of 14.2 ± 0.6 µm (10 microwires), 23.5 ± 1.0 µm (6 microwires) or 118 ± 4 µm (2 microwires). A second series of higher 99.999% purity (5N) aluminium microwires were produced similarly, with a diameter of 23.5 ± 1.3 µm (4 microwires) or 116 ± 4 µm (5 microwires). Only microwires with a regular cross-section along their complete gauge length (~1.5 mm) were retained for testing. Fig. 2 shows a portion of as-cast microwires in each of the three different diameter ranges. Using atomic force microscopy scans along the surface of three undeformed microwires, the root mean square roughness was found to be 5.2 ± 1.2 nm.

Tensile curves of the 4N and 5N Al microwires are given in Figs. 3 and 4, respectively. Plots are separated based on the microwire diameter and the horizontal axis gives the microwire plastic shear strain. The onset of each stress relaxation is marked by an inverted (black) triangle along the stress-strain curve. The initial crystallographic orientation of each microwire is shown in the accompanying standard stereographic triangle. Coloured arrows are added above the curves to mark the strain where the upper envelope of the stress-strain curve features an inflexion point.

All deformed microwires show slip steps along their surface; Fig. 3d gives an example. The density and visual aspect of those slip steps vary overall as expected given the initial crystallographic orientation of the microwires, namely: (i) wires oriented for single slip show clearly visible slip steps corresponding to one predominant glide system, while (ii) several glide systems are generally visible along wires initially oriented for multiple slip. Fewer and smaller steps are visible along the surface of the sample oriented along <111>, denoting that this sample has deformed in nearly

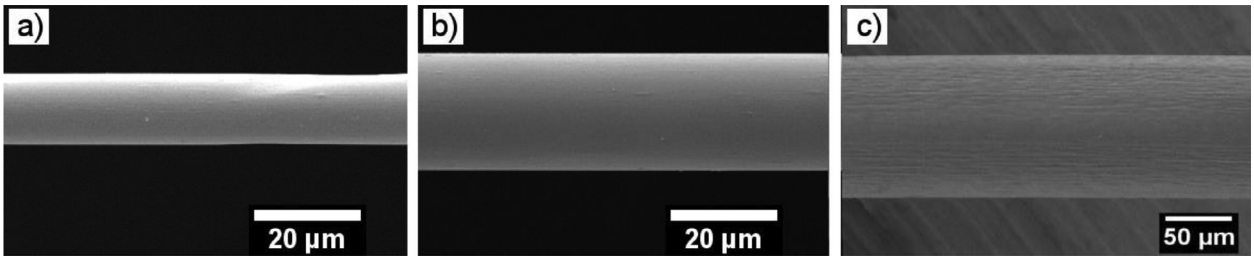

Fig. 2. SEM images of undeformed 4N microwires of diameter (a) 13.2 µm, (b) 21.6 µm and (c) 107 µm.

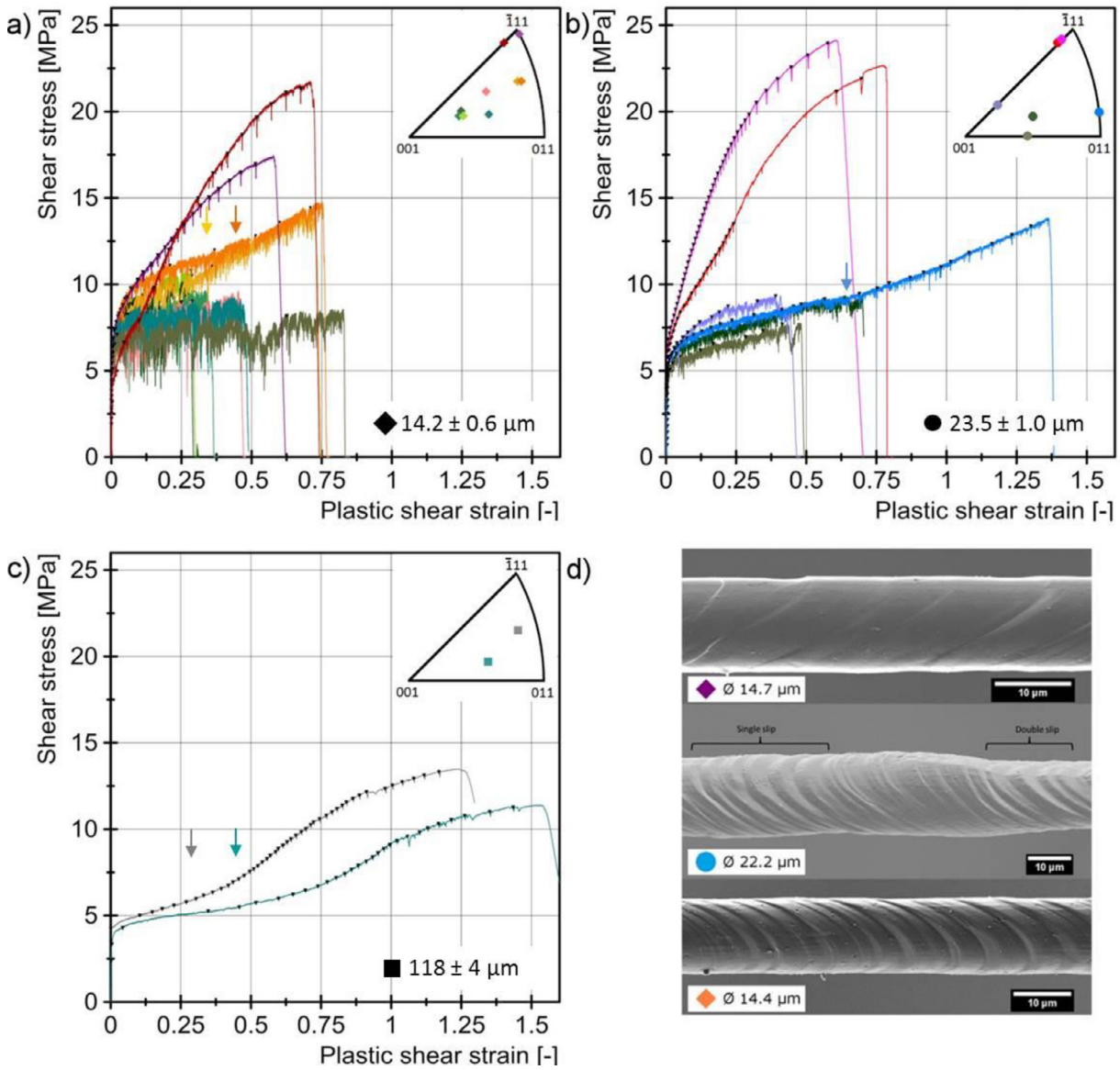

Fig. 3. Resolved plastic shear strain-shear stress curve of aluminium (4N) microwires with a diameter in the range (a) 12.7–14.7 µm ("~14 µm"), (b) 22.2–25.0 µm ("~22 µm") and (c) 115–121 µm ("~115 µm"). Triangles denote the onset of relaxation events; arrows denote an inflexion point in the upper envelope of the curve. (d) Portion of deformed microwires oriented (from top to bottom) for multiple slip, coplanar double slip or single slip.

uniform fashion. Exception made for the neck region, secondary slip steps are essentially absent along the surface of 4N Al microwires oriented for single slip, see Fig. 3d (and Supplementary Information Figs. S1 and S2). The 5N Al microwires oriented for single slip, which reached higher strains before failing than did 4N pure microwires, show in post-mortem SEM examination the presence of a few secondary slip steps along their surface in addition to those corresponding to the primary slip system (see Supplementary Information Figs. S3 and S4).

During a stress relaxation hold, while the stress decreases, the deformation of aluminium microwires combines periods of continuous deformation interrupted by sudden displacement events. From each stress relaxation, an apparent activation area was extracted (as described in Section 2.3 and in Ref. [30]).

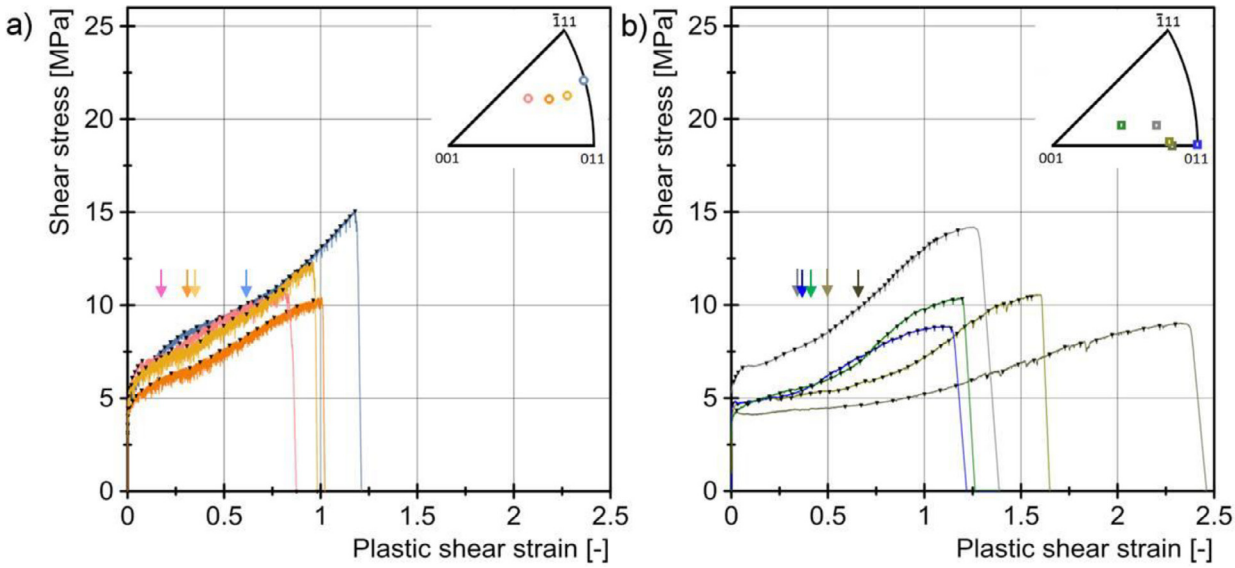

Fig. 4. Resolved plastic shear strain-shear stress curve of aluminium (5N) microwires with a diameter in the range (a) 21.6–24.3 µm ("~22 µm") and (b) 112–125 µm ("~115 µm") respectively. Triangles denote the onset of relaxation events; arrows denote an inflexion point in the upper envelope of the curve.

In Figs. 5 and 6 the inverse of the (dimensionless) measured apparent activation area (b^2/a) values are plotted in the coordinates of a Haasen plot [47–49] for the 4N and 5N wires, respectively. In the figures, the data are separated based on the wire diameter and the number of slip systems activated in the wire upon its initial deformation.

4. Discussion

4.1. Tensile behaviour

The tensile deformation of the microcast Al 99.99% wires is consistent with what is observed in prior studies; see Refs. [9,29,72]. The yield stress varies, within significant scatter, roughly as the inverse of the wire diameter (see Fig. 2 of Ref. [29]), and the displacement burst intensity cumulative distribution functions are similar to those measured during monotonic wire testing [8] (those curves are given in Ref. [72]). There is furthermore no measurable difference in plastic deformation behaviour (flow stress, curve shape, dependence on the crystallographic orientation or the microwire diameter) that can be linked with the metal purity of the microwires; compare (i) the dark green curve in Fig. 3b to the yellow and orange curves in Fig. 4a; (ii) blue curves across Figs. 3b and 4a, or (iii) curves in Figs. 3c and 4b. The only discernible difference is a somewhat higher strain to failure (*i.e.,* a greater deformation range; note the difference in strain scale between Figs. 3 and 4) for 5N Al microwires compared to 4N Al microwires. Impurities present in the 4N aluminium thus exert little influence on the plastic deformation of the present microwires.

Aluminium microwires with a diameter >100 µm were all oriented for single slip. Their plastic deformation shows the three classical stages of FCC monocrystal deformation (Figs. 3c and 4b), with the transition from Stage I to Stage II relatively well captured by the inflexion point (see arrows over the curves) [63,73]. The main noticeable difference compared with (macroscopic) aluminium bulk crystals [63,73] is that the present microwires show more extended Stages I and II. This observation is consistent with early work on single crystalline copper crystals of diameter down to 100 µm [64,74].

Contrary to their larger >100 µm diameter counterparts (and to bulk aluminium crystals), the single slip oriented microwires with D~14–25 µm, Figs. 3a,b and 4a, do not display deformation stage transitions that are as clear as those seen with larger wires or with bulk crystals. Examination of their post-mortem wire surface reveals that their deformation proceeded essentially in single slip, see Fig. 4d and figures in the Supplementary Information. The predominance of single slip (Stage I) deformation in those samples agrees with the relatively high strain at which the upper envelope of the tensile curve of those samples shows an inflection point, Figs. 3a,b and 4a. It also agrees with the comparatively low rate of work hardening of those wires, on the order of 5 MPa, or G/5000, typical of Stage I deformation of FCC single crystals [75,76].

Thinner microwires (D~14–25 µm) oriented near the multiple-slip <111> direction deform with a higher rate of work hardening, Fig. 3a,b, and tend to display far fewer and much shallower slip steps along their surface, Fig. 3d. Two microwires oriented for coplanar double slip were also tested (one of each metal purity, Figs. 3b and 4a). This is a metastable orientation: two different slip systems with a common slip plane, or alternatively only one of those two slip systems, is initially activated in such wires [1]. SEM images of the deformed microwires show in some locations that separate regions have deformed differently within the same wire cross-section, giving it a heart-shaped cross-section after deformation (Fig. 3d; see also Figs. S1 and S3 in the Supplementary Information). Tensile curves of those microwires show a long region of low work hardening rate before the inflexion point is observed, Figs. 3b and 4a.

4.2. Thermally activated deformation

That intermittent plastic deformation also occurs during stress relaxation implies that thermal activation can aid the mechanism that initiates sudden displacement events, even though the applied stress is steadily decreasing to values lower than the instantaneous flow stress. This agrees with findings of Ng and Ngan [31] who have reported that sudden displacement jumps occur during creep holds in compression-tested ion-milled aluminium micropillars.

From the continuous part of each single stress relaxation an apparent activation area a can be measured once the effect of sudden displacement jumps is removed as described in Section 2.2. The resulting activation area is tagged here as "apparent", in keeping with the terminology of Ref. [49] and also because we could not perform repeated stress relaxations [67,77,78], for two reasons. The first is the presence of the sudden displacement jumps also dur-

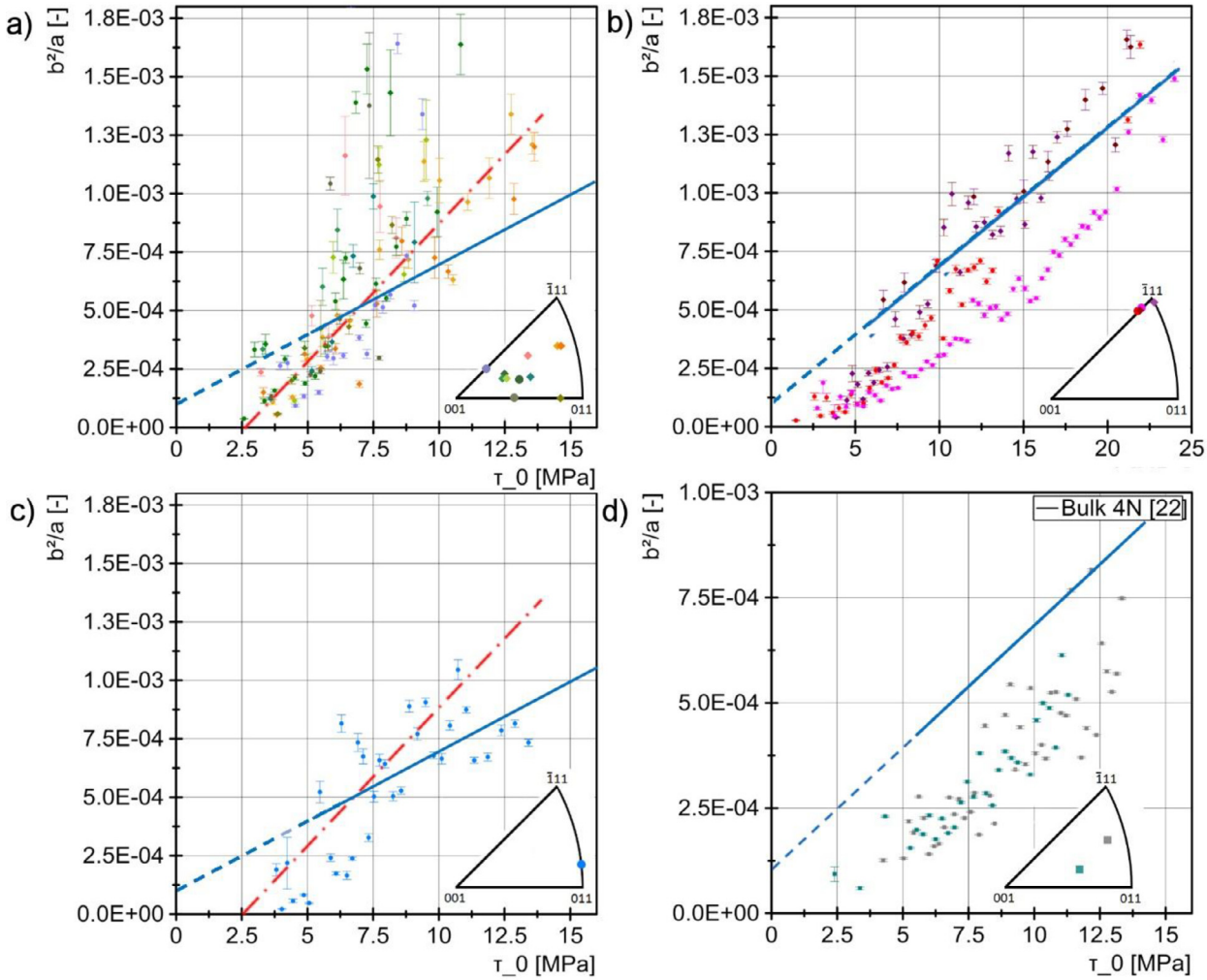

Fig. 5. Haasen plot of Al4N microwires (a) oriented for single slip, (b) oriented for multiple slip (note the different scale) and (c) oriented for metastable double slip; (d) gives data for thick (>100 μm) microwires oriented for single slip, plotted together with (blue) line for data for the same 4N aluminium in bulk form from Ref. [46]. Red line is a line with twice the slope of the blue line that intercepts the stress axis at 2.5 MPa.

ing reloading, which makes it difficult to reload the samples quasi-elastically. The second difficulty is that it is nearly impossible to produce repeated relaxations of equal amplitude, either in terms of stress amplitude (since jumps are sudden and of unknown size) or in terms of strain amplitude (given the variability, after elimination of jumps, of the strain range covered by continuous processes during each 60 s long relaxation). We therefore make do here with single relaxation testing. We are, however, entitled to expect that single and repeated relaxation testing will give similar results in present samples, by drawing on an earlier study of the thermally activated deformation behaviour of compression samples made of the same 4N aluminium as was used here, in (i) bulk cold-rolled and annealed form, and also (ii) in open pore microcellular form produced by replication, a process close to that used here (namely, pressure infiltration of the molten metal into a preform of packed NaCl powder, which was then removed by leaching in the same chromate solution) [46]. In replicated microcellular 4N aluminium, individual struts are also monocrystalline and can be made to have a diameter similar to that of the microwires studied here. It was found that the load relaxation signal is smooth both for the dense and for the microcellular metal (where signal emanates from many thousand struts deforming simultaneously). For both 4N aluminium (bulk and microcellular) sample types, repeated stress relaxation tests were possible: activation areas captured respectively by repeated and single relaxation testing were measured and found to be essentially the same. This lends credence to our assumption that the difference is likely to be negligible also in the present microwires.

As mentioned above, Haasen plots are a convenient and enlightening way to interpret activation area data: the plot carries, in its shape, intercept and slope, information on the mechanism(s) ruling thermal activation. The plot is linear and passes through the origin for a single phase material free of back-stress and in which only simple forest dislocation-to-dislocation interactions control plastic flow [48,79]. The slope of the line then equals ($b^3/\Delta W'$) where $\Delta W'$ is the (*apparent* in the terminology of Ref. [49]) work done by the applied stress in aiding dislocations overcome obstacles with assistance from thermal activation [46,49]. The Haasen plot can also give information when more than one type of obstacle contributes to the measured flow stress [48,49]. The linear relationship is maintained for systems with one additional type of obstacle if the contribution to the flow stress of both obstacles is additive and they have a very different strength or density. If the second type of obstacle is more rate-sensitive (*e.g.*, solid solution atoms) then the Haasen plot is shifted upwards, giving it a positive intercept with the y-axis. In contrast, if there is a constant athermal

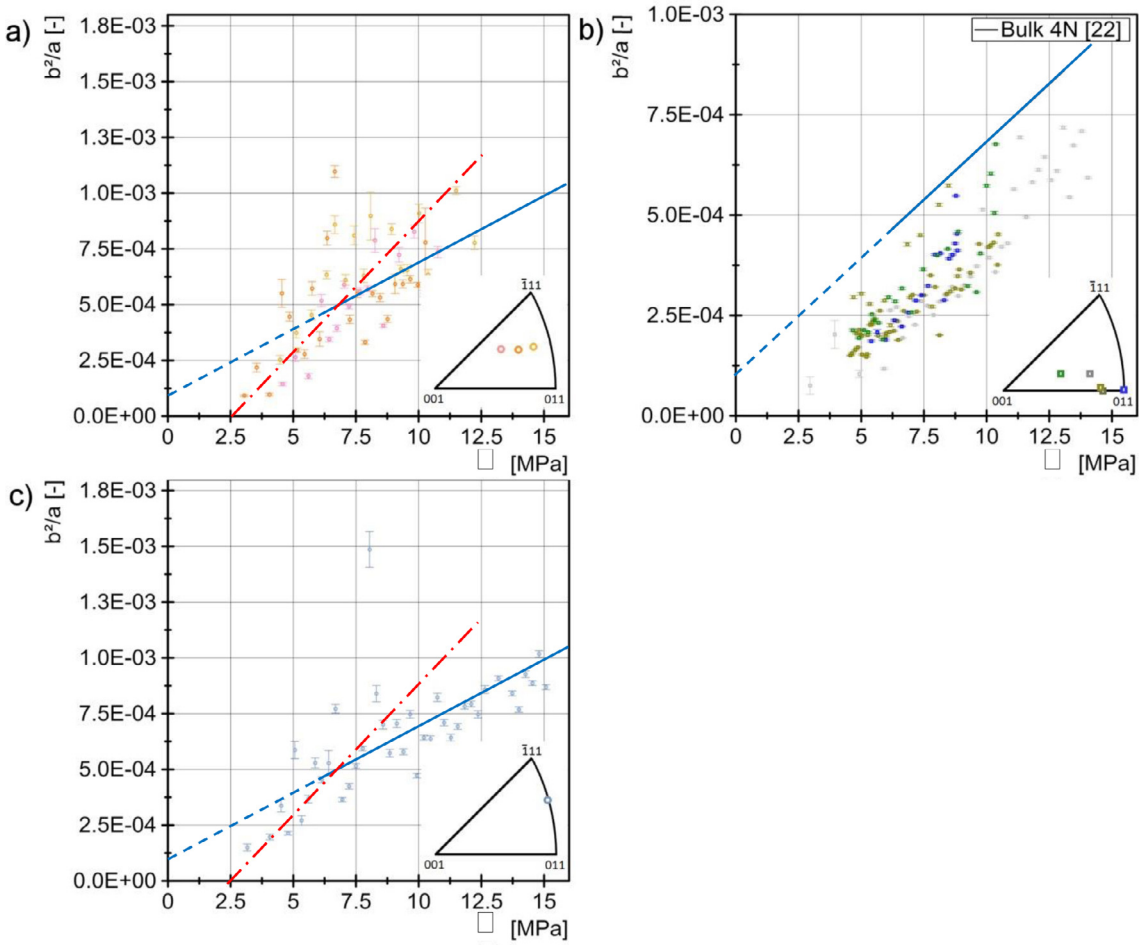

Fig. 6. Haasen plots of Al5N microwires; (a) ~22 µm diameter samples oriented for single slip, (b) ~115 µm diameter samples oriented for single slip and (c) ~22 µm diameter sample oriented for metastable double slip. Blue line is a linear fit of data for the same 4N aluminium in bulk form from Diologent et al., Ref. [46]; red dash-dot line has twice the slope of the blue line.

contribution to the flow stress (meaning a fixed back-stress) this results in a line that has a positive intercept with the horizontal (stress) axis [48,49,79].

Figs. 5 and 6 show the measured Haasen plots of the Al4N and Al5N microwires, respectively, with data combined according to the metal purity and the number of activated slip systems upon initial deformation. On the plots in both figures the continuous blue line corresponds to the line that fits through data of Ref. [46] for the same 4N aluminium metal in bulk form tested after rolling and annealing. The line is extended in dotted form to zero stress, and plotted in present graphs after conversion of tensile stress values of Ref. [46] to resolved shear stress data using the Taylor factor (3.06). The following observations emerge:

(1) Data points from each of the 4N aluminium 14–25 µm diameter samples having their axis oriented near the <111> direction, Fig. 5b, align relatively well along a straight line that has roughly the same slope as data for the same metal in bulk form, save for a shift to the right, suggesting the presence of a (resolved shear) back-stress in the range 0–5 MPa.
(2) The same can be said for larger samples, of diameter near 100 µm, whether cast of 4N (Fig. 5d) or 5N (Fig. 6b) aluminium.
(3) 14–25 µm diameter samples oriented for single slip (Figs. 5a and 6a) show a far higher degree of scatter, so much so that one cannot say (without some form of data averaging) that they delineate a straight line. Overall, as found for multislip or 100 µm diameter samples, data tend to converge to meet the horizontal (stress) axis at $\tau_o = 2.5$ MPa, suggesting the presence of a back-stress having that value. The values and overall rate of increase of b^2/a with the flow stress are higher than shown by the blue line, i.e., than is observed for bulk aluminium and for multislip or 100 µm diameter samples of this work. Rather, the trend is toward a rate of increase of b^2/a with stress that is twice as high if not steeper. To guide the eye we have added to the figures a dash-dotted red line that has a slope twice that of the blue (bulk Al) line and cuts the horizontal axis at $\tau_o = 2.5$ MPa.
(4) The 14-25 µm diameter sample oriented along the <011> - <111> line (Fig. 5c), which deforms by unstable double slip, also shows highly scattered and somewhat more steeply rising data, compared to the bulk metal (blue line), at lower resolved stress values ($\tau \leq 7.5$ MPa). At higher stress values data then remain relatively close on average to the line for bulk aluminium. The data also cut the abscissa axis at $\tau_o \approx 2.5$ MPa. The behaviour of those microcast crystals is thus intermediate between that of samples of the same size that are (i) oriented for single slip and (ii) those that are oriented near <111>, i.e., for (stable) multiple slip.
(5) Finally, there is no noticeable systematic difference between data for 4N and 5N purity aluminium. This implies that impurities, known to potentially affect, even at low concentrations, plasticity in unalloyed metal deformation (e.g., [51,61,80,81]), are here of no consequence.

Compared with single-crystalline aluminium data of Ref. [34], activation volumes (or areas) measured in this work tend to be

somewhat higher (nearer 1000 b^3 than 100 b^3); however, this is in part due to the different reference stress used (the von-Mises stress in Ref. [34], the resolved shear stress in the present work). Present data do not fit a trend according to which the strain-rate sensitivity of the flow stress (and with it the inverse of the activation area) increases as the samples diameter decreases; rather, the dependence on flow stress, and hence on the overall plastic strain, is stronger than any noticeable systematic size-dependence of a, see Figs. 5 and 6.

The positive intercept in the Haasen plots with the x-axis near $\tau_o = 2.5$ MPa reveals the presence of an athermal contribution to the flow stress, *i.e.*, of a back-stress. In the present microwires, such a back-stress has a likely origin, namely the thin oxide layer that lines the microwire surface. Oxide is always present along the surface of aluminium, including in aluminium dissolved from an NaCl mould in a chromate-solution [82]. The actual thickness of the oxide layer on the present microwires was not measured; however, by analogy with observations in Ref. [82] for replicated 4N aluminium leached from its NaCl mould using the same chromate solution as was used here, we expect an oxide layer with a thickness of <10 nm to line the surface of the microcast wires. Such a thin oxide layer is not load-bearing: the uniform (elastic) strain of the microwire as it deforms is on average $\approx 2\bullet 10^{-4}$. A quick calculation of the force exerted by the oxide layer when deformed elastically up to such strains, assuming a thickness of 10 nm and a Young's modulus of 370 GPa [83] gives for the thinnest wires ($D = 14$ µm) a force in the cross-section of the order of 30 µN. This is negligible compared with the total load carried by the plastically deforming microwire of similar diameter (>1 mN). The oxide layer (which in addition does not support large tensile strains before cracking) will thus not shift the wires' flow stress much by direct load-bearing. The back-stress is therefore likely caused by the well-known capacity of the oxide layer to block or hinder the escape of dislocations through the surface of aluminium crystals (a 10 nm thick alumina layer of – moderate - shear strength 1 GPa can withstand a linear shear force of 10 N/m, which is well above the shear force exerted by dislocations moving in the present crystals). That the oxide layer covering the wires is the source of this back stress is confirmed by data from similar wires after annealing, where the back-stress and the flow stress both increase after growth of the oxide, causing Haasen plot data of two annealed samples similar to those of this work to shift towards the right and intersect the horizontal (stress) axis near $\tau_o = 9.5$ MPa [29,30].

Two aspects of the present data are the most intriguing, namely that, in thinner microcast crystals oriented for single slip, (i) the scatter is far higher, and (ii) the average rate of increase of b^2/a with τ is noticeably steeper than data for the metal in bulk form, or in other samples of this work (multiple slip-oriented or larger microcast crystals), Figs. 5 and 6.

The scatter can be explained by the fact that deformation along the wires is highly inhomogeneous, particularly when they are oriented for single slip. Differences in the local environment of dislocation sources can therefore be invoked to explain differences in individual measured activation area values gleaned from relaxation curves that are, each, likely to be driven by a limited number of significantly different discrete dislocation sources within the wire.

The steeper rate of increase of b^2/a with τ bears resemblance with (i) similar observations in crystals of FCC metal upon the transition from Stage I (single slip) to Stage II deformation that can be found in some of the older literature (where it is typically referred to as a small-strain deviation from the Cottrell-Stokes law) [58,60,62], and (ii) to data from replicated microcellular aluminium made of the same 4N metal [46]. The latter data (Fig. 7 of Ref. [46]) align along straight lines, with a $\Delta W'$ decreased by half (and hence a slope twice as high) when the diameter of the (monocrystalline) deforming struts falls below roughly 25 µm, compared with coarser microcellular metal struts, which give $\Delta W'$ values similar to what is measured on the same 4N aluminium metal in bulk form. The same halving of $\Delta W'$ was also observed for an Al-5 wt. pct. Mg alloy in microcellular form [46]. The red dash-dotted line (situated so as to intercept the x-axis at $\tau_o = 2.5$ MPa) in Figs. 5a,c and 6a has a slope twice that of the blue line for bulk pure aluminium and thus corresponds to data for the finer microcellular structures of Ref. [46]: that line captures better the initial rate of increase of b^2/a with τ than does the blue line. A steeper rate of increase of b^2/a with τ than is shown by the blue line or by data in Figs. 5b,d and 6b is also suggested (but with an offset to intercept the horizontal axis at $\tau_o = 9.5$ MPa) by the data for two similar but annealed wires; see Fig. 4 of Ref. [29].

The explanation that was offered in Ref. [46][1] to explain why $\Delta W'$ is halved in finer microcellular metal struts might therefore apply here. It was proposed in Ref. [46] that near a free surface image forces might effectively duplicate (virtually, across the free surface) the operating dislocation obstacle bypass mechanism. This would cause in turn the work effectively contributed by the applied stress as the dislocation overcomes obstacles situated at, or near, the strut surface to be halved; however, if that mechanism were the underlying cause in the present samples then it should pertain regardless of microwire orientation – which is contradicted by present data since it is not observed in multislip.

Why then is there a decrease, by a factor near two, of $\Delta W'$ in thinner aluminium single crystals when they deform in single slip near a free surface ? The operative mechanism must have the following features: (i) it must be specific to easy glide (Stage I, single slip), (ii) it must be specific to small-scale samples or in other words it must operate near a free surface (since it is not observed in 100 µm wires oriented for single-glide nor in coarser, 400 µm diameter pore, microcellular aluminium), (iii) it must operate also in the presence of solution hardening (since it also obtains in fine-scale Al-5wt%Mg).

It is known that in bulk aluminium both the flow stress and the measured activation area values are consistent with the Taylor equation assuming an interaction strength (α) value of 0.3 [1,84]. This consistency between flow stress and activation area values is in accord with data for present microwires when they deform in multiple slip [9,29,72,85]. Present data suggest that, when aluminium deforms in easy glide near a free surface, this consistency is broken in a way that lowers $\Delta W'$ by a factor near two. TEM data [51,64,84,86–90], theoretical analysis [62,91,92] and 3D dislocation dynamics simulations [9,84,93,94] show that in easy glide FCC crystals contain long braids of parallel multipolar groups of edge dislocations lying along the glide plane and intersected by, or connected to, superjogs, with which they interlock via the (strong) colinear interaction. Documenting how a free surface interacts with those structures is beyond the scope of this work, if only because detailed TEM observations would be required. One possibility is that image forces, exerted either on gliding edge segments intersecting the free surface or on superjogs in their vicinity, amplify the contribution of the applied stress toward reducing the activation energy required for a gliding dislocation to bypass threading superjogs or other forest dislocations along their glide path. Such a mechanism would be consistent with the strong influence that is exerted by free surfaces on Stage I dislocation glide (*e.g.*, [95–98]), and would indeed alter the otherwise observed coupling of the measured activation area with the resolved shear flow stress.

[1] Footnote: in the last line of p. 6877 of Ref. [46], the word "halving" should be converted to "doubling".

5. Conclusion

Microcast aluminium microwires of 99.99 and 99.999% pure Al with a diameter of ∼14, 25 and 115 µm and having different crystalline orientations are tested in tension with periodic 60 s stress relaxations. The plastic deformation behaviour of the microwires is strongly influenced by both their diameter and their orientation. It is on the other hand not altered by an increase in metal purity from 99.99 to 99.999% pure Al, leading to conclude that impurities do not affect the deformation of the 4N aluminium used here or in Refs. [9,29,30,46,82,85].

Intermittent plasticity is observed in all microwires of this work and accounts for a significant fraction of the total plastic deformation when microwires deform by single slip. Such intermittency is also observed during stress relaxation, while the applied stress decreases. Data collected during relaxation events show, within greater scatter, no marked departure from data collected during monotonic deformation, other than the fact that sudden strain bursts are less frequently initiated when the applied stress falls below the instantaneous flow stress of the metal.

Separating the continuous part from the intermittent part of the load signal during stress relaxation, apparent activation area values are measured for processes that cause continuous, non-intermittent, wire deformation. Collecting results in Haasen plots shows that, for small ($D \leq 25$ µm) microwires deforming in single slip, b^2/a data are more highly scattered and increase more steeply, by a factor near two, with the flow stress compared to what is documented for (i) similar wires in multiple slip, (ii) larger (D ∼100 µm) microwires, or (iii) the bulk metal. The steeper increase observed when smaller microwires deform by single slip parallels what is observed in microcellular aluminium when the pore size is sufficiently small for metal struts to have a diameter on the order of 25 µm or below; likely the same size-effect operates in both. Present data thus show that it is when micron-scale aluminium deforms by easy glide that the thermal activation of dislocation motion driving continuous plastic deformation departs from bulk behaviour, to show a reduction by a factor near two of the apparent work done by the resolved applied stress in overcoming obstacles to dislocation motion.

Declaration of Competing Interest

The authors declare that they have no known competing financial interests or personal relationships that could have appeared to influence the work reported in this paper.

Acknowledgments

This research was funded by the Swiss National Science Foundation, Project 200020_156054/1. The authors thank Dr. Kurt Schenk at EPFL who measured the orientation of our microwires using monocrystalline diffraction. We also gratefully acknowledge many interesting discussions of this work (while the authors of course bear full responsibility for its content and interpretation) with Dr. Ladislas Kubin, Dr. Marc Legros, Dr. Satish Rao, Prof. Erica Lilleodden and Prof. William Curtin.

Supplementary materials

Supplementary material associated with this article can be found, in the online version, at doi:10.1016/j.actamat.2022.118037.

References

[1] L.P. Kubin, Dislocations, Mesoscale Simulations and Plastic Flow, 1st ed., Oxford Univsity Press, 2013.
[2] J.R. Greer, J.T.M. De Hosson, Plasticity in small-sized metallic systems: intrinsic versus extrinsic size effect, Prog. Mater. Sci. 56 (2011) 654–724, doi:10.1016/j.pmatsci.2011.01.005.
[3] G. Dehm, B.N. Jaya, R. Raghavan, C. Kirchlechner, Overview on micro- and nanomechanical testing: new insights in interface plasticity and fracture at small length scales, Acta Mater. 142 (2018) 248–282, doi:10.1016/j.actamat.2017.06.019.
[4] J.A. El-Awady, Unravelling the physics of size-dependent dislocation-mediated plasticity, Nat. Commun. 6 (2015) 5926, doi:10.1038/ncomms6926.
[5] Yu.I. Golovin, Nanoindentation and mechanical properties of materials at submicro- and nanoscale levels: recent results and achievements, Phys. Solid State 63 (2021) 1–41, doi:10.1134/S1063783421010108.
[6] H. Bei, S. Shim, G.M. Pharr, E.P. George, Effects of pre-strain on the compressive stress–strain response of Mo-alloy single-crystal micropillars, Acta Mater. 56 (2008) 4762–4770, doi:10.1016/j.actamat.2008.05.030.
[7] T.A. Parthasarathy, S.I. Rao, D.M. Dimiduk, M.D. Uchic, D.R. Trinkle, Contribution to size effect of yield strength from the stochastics of dislocation source lengths in finite samples, Scr. Mater. 56 (2007) 313–316, doi:10.1016/j.scriptamat.2006.09.016.
[8] S.I. Rao, D.M. Dimiduk, T.A. Parthasarathy, M.D. Uchic, M. Tang, C. Woodward, Athermal mechanisms of size-dependent crystal flow gleaned from three-dimensional discrete dislocation simulations, Acta Mater. 56 (2008) 3245–3259, doi:10.1016/j.actamat.2008.03.011.
[9] J. Krebs, S.I. Rao, S. Verheyden, C. Miko, R. Goodall, W.A. Curtin, A. Mortensen, Cast aluminium single crystals cross the threshold from bulk to size-dependent stochastic plasticity, Nat. Mater. (2017), doi:10.1038/nmat4911.
[10] M.D. Uchic, Sample dimensions influence strength and crystal plasticity, Science 305 (2004) 986–989, doi:10.1126/science.1098993.
[11] V.S. Deshpande, A. Needleman, E. Van der Giessen, Plasticity size effects in tension and compression of single crystals, J. Mech. Phys. Solids 53 (2005) 2661–2691, doi:10.1016/j.jmps.2005.07.005.
[12] G. Dehm, Miniaturized single-crystalline FCC metals deformed in tension: new insights in size-dependent plasticity, Prog. Mater. Sci. 54 (2009) 664–688, doi:10.1016/j.pmatsci.2009.03.005.
[13] D. Kiener, C. Motz, G. Dehm, Micro-compression testing: a critical discussion of experimental constraints, Mater. Sci. Eng. A 505 (2009) 79–87, doi:10.1016/j.msea.2009.01.005.
[14] D. Kiener, W. Grosinger, G. Dehm, On the importance of sample compliance in uniaxial microtesting, Scr. Mater. 60 (2009) 148–151, doi:10.1016/j.scriptamat.2008.09.024.
[15] D. Kiener, C. Motz, M. Rester, M. Jenko, G. Dehm, FIB damage of Cu and possible consequences for miniaturized mechanical tests, Mater. Sci. Eng. A 459 (2007) 262–272, doi:10.1016/j.msea.2007.01.046.
[16] J. Hütsch, E.T. Lilleodden, The influence of focused-ion beam preparation technique on microcompression investigations: Lathe vs. annular milling, Scr. Mater. 77 (2014) 49–51, doi:10.1016/j.scriptamat.2014.01.016.
[17] Y. Xiao, J. Wehrs, H. Ma, T. Al-Samman, S. Korte-Kerzel, M. Göken, J. Michler, R. Spolenak, J.M. Wheeler, Investigation of the deformation behavior of aluminum micropillars produced by focused ion beam machining using Ga and Xe ions, Scr. Mater. 127 (2017) 191–194, doi:10.1016/j.scriptamat.2016.08.028.
[18] M. Chen, J. Wehrs, A.S. Sologubenko, J. Rabier, J. Michler, J.M. Wheeler, Size-dependent plasticity and activation parameters of lithographically-produced silicon micropillars, Mater. Des. 189 (2020) 108506, doi:10.1016/j.matdes.2020.108506.
[19] J. Liu, R. Niu, J. Gu, M. Cabral, M. Song, X. Liao, Effect of ion irradiation introduced by focused ion-beam milling on the mechanical behaviour of sub-micron-sized samples, Sci. Rep. 10 (2020) 10324, doi:10.1038/s41598-020-66564-y.
[20] F. Mompiou, M. Legros, Plasticity mechanisms in sub-micron Al fiber investigated by *in situ* TEM, Adv. Eng. Mater. 14 (2012) 955–959, doi:10.1002/adem.201200020.
[21] H. Bei, E.P. George, Microstructures and mechanical properties of a directionally solidified NiAl–Mo eutectic alloy, Acta Mater. 53 (2005) 69–77, doi:10.1016/j.actamat.2004.09.003.
[22] A.T. Jennings, M.J. Burek, J.R. Greer, Microstructure versus size: mechanical properties of electroplated single crystalline Cu nanopillars, Phys. Rev. Lett. 104 (2010), doi:10.1103/PhysRevLett.104.135503.
[23] G. Lee, J.Y. Kim, A.S. Budiman, N. Tamura, M. Kunz, K. Chen, M.J. Burek, J.R. Greer, T.Y. Tsui, Fabrication, structure and mechanical properties of indium nanopillars, Acta Mater. 58 (2010) 1361–1368, doi:10.1016/j.actamat.2009.10.042.
[24] M.J. Burek, S. Jin, M.C. Leung, Z. Jahed, J. Wu, A.S. Budiman, N. Tamura, M. Kunz, T.Y. Tsui, Grain boundary effects on the mechanical properties of bismuth nanostructures, Acta Mater. 59 (2011) 4709–4718, doi:10.1016/j.actamat.2011.04.017.
[25] A.S. Budiman, G. Lee, M.J. Burek, D. Jang, S.M.J. Han, N. Tamura, M. Kunz, J.R. Greer, T.Y. Tsui, Plasticity of indium nanostructures as revealed by synchrotron X-ray microdiffraction, Mater. Sci. Eng. A 538 (2012) 89–97, doi:10.1016/j.msea.2012.01.017.
[26] A.T. Jennings, J. Li, J.R. Greer, Emergence of strain-rate sensitivity in Cu nanopillars: transition from dislocation multiplication to dislocation nucleation, Acta Mater. 59 (2011) 5627–5637, doi:10.1016/j.actamat.2011.05.038.
[27] S. Buzzi, M. Dietiker, K. Kunze, R. Spolenak, J.F. Löffler, Deformation behavior of silver submicrometer-pillars prepared by nanoimprinting, Philos. Mag. 89 (2009) 869–884, doi:10.1080/14786430902791748.

[28] M. Dietiker, S. Buzzi, G. Pigozzi, J.F. Löffler, R. Spolenak, Deformation behavior of gold nano-pillars prepared by nanoimprinting and focused ion-beam milling, Acta Mater. 59 (2011) 2180–2192, doi:10.1016/j.actamat.2010.12.019.
[29] S. Verheyden, L. Pires Da Veiga, L. Deillon, A. Mortensen, The effect of size on the plastic deformation of annealed cast aluminium microwires, Scr. Mater. 161 (2019) 58–61, doi:10.1016/j.scriptamat.2018.10.009.
[30] S. Verheyden, L. Deillon, A. Mortensen, Stress relaxation in the presence of sudden strain bursts: methodology and stress relaxation data of microcast aluminium microwires, Data Brief 21 (2018) 2134–2141, doi:10.1016/j.dib.2018.11.047.
[31] K.S. Ng, A.H.W. Ngan, Creep of micron-sized aluminium columns, Philos. Mag. Lett. 87 (2007) 967–977, doi:10.1080/09500830701666147.
[32] V. Maier-Kiener, K. Durst, Advanced nanoindentation testing for studying strain-rate sensitivity and activation volume, JOM 69 (2017) 2246–2255, doi:10.1007/s11837-017-2536-y.
[33] K. Durst, V. Maier, Dynamic nanoindentation testing for studying thermally activated processes from single to nanocrystalline metals, Curr. Opin. Solid State Mater. Sci. 19 (2015) 340–353, doi:10.1016/j.cossms.2015.02.001.
[34] Y. Xiao, V. Maier-Kiener, J. Michler, R. Spolenak, J.M. Wheeler, Deformation behavior of aluminum pillars produced by Xe and Ga focused ion beams: insights from strain rate jump tests, Mater. Des. 181 (2019) 107914, doi:10.1016/j.matdes.2019.107914.
[35] Y. Xiao, R. Kozak, M.J.R. Haché, W. Steurer, R. Spolenak, J.M. Wheeler, Y. Zou, Micro-compression studies of face-centered cubic and body-centered cubic high-entropy alloys: size-dependent strength, strain rate sensitivity, and activation volumes, Mater. Sci. Eng. A 790 (2020) 139429, doi:10.1016/j.msea.2020.139429.
[36] S. Guo, Y. He, Z. Li, J. Lei, D. Liu, Size and stress dependences in the tensile stress relaxation of thin copper wires at room temperature, Int. J. Plast. 112 (2019) 278–296, doi:10.1016/j.ijplas.2018.09.001.
[37] G. Mohanty, J.M. Wheeler, R. Raghavan, J. Wehrs, M. Hasegawa, S. Mischler, L. Philippe, J. Michler, Elevated temperature, strain rate jump microcompression of nanocrystalline nickel, Philos. Mag. 95 (2015) 1878–1895, doi:10.1080/14786435.2014.951709.
[38] J.M. Wheeler, L. Thilly, A. Morel, A.A. Taylor, A. Montagne, R. Ghisleni, J. Michler, The plasticity of indium antimonide: insights from variable temperature, strain rate jump micro-compression testing, Acta Mater. 106 (2016) 283–289, doi:10.1016/j.actamat.2015.12.036.
[39] G. Mohanty, J. Wehrs, B.L. Boyce, A. Taylor, M. Hasegawa, L. Philippe, J. Michler, Room temperature stress relaxation in nanocrystalline Ni measured by micropillar compression and miniature tension, J. Mater. Res. 31 (2016) 1085–1095, doi:10.1557/jmr.2016.101.
[40] J. Wehrs, M.J. Deckarm, J.M. Wheeler, X. Maeder, R. Birringer, S. Mischler, J. Michler, Elevated temperature, micro-compression transient plasticity tests on nanocrystalline palladium-gold: probing activation parameters at the lower limit of crystallinity, Acta Mater. 129 (2017) 124–137, doi:10.1016/j.actamat.2017.02.045.
[41] Y. Xiao, Y. Zou, A.S. Sologubenko, R. Spolenak, J.M. Wheeler, Size-dependent strengthening in multi-principal element, face-centered cubic alloys, Mater. Des. 193 (2020) 108786, doi:10.1016/j.matdes.2020.108786.
[42] M. Chen, J. Wehrs, A.S. Sologubenko, J. Rabier, J. Michler, J.M. Wheeler, Size-dependent plasticity and activation parameters of lithographically-produced silicon micropillars, Mater. Des. 189 (2020) 108506, doi:10.1016/j.matdes.2020.108506.
[43] Y. Xiao, B. Gan, A.S. Sologubenko, R. Spolenak, J.M. Wheeler, Size- and strain rate-dependence of nickel and Ni–Co micropillars with varying stacking fault energy, Mater. Sci. Eng. A 800 (2021) 140266, doi:10.1016/j.msea.2020.140266.
[44] H. Li, T. Zhu, N. Takata, M. Kobashi, M. Yoshino, Thermal activation process of plastic deformation in Fe–18Cr single-crystal micropillars with high-density dislocations, Mater. Sci. Eng. A 819 (2021) 141459, doi:10.1016/j.msea.2021.141459.
[45] H. Li, T. Zhu, N. Takata, M. Kobashi, M. Yoshino, Effect of trace solute titanium on plastic deformation of α-(Fe, Cr) single-crystal micropillars fabricated from 18Cr ferritic stainless steel, Mater. Sci. Eng. A 803 (2021) 140455, doi:10.1016/j.msea.2020.140455.
[46] F. Diologent, R. Goodall, A. Mortensen, Activation volume in microcellular aluminium: size effects in thermally activated plastic flow, Acta Mater. 59 (2011) 6869–6879, doi:10.1016/j.actamat.2011.07.021.
[47] P. Haasen, Plastic deformation of nickel single crystals at low temperatures, Philos. Mag. 3 (1958) 384–418, doi:10.1080/14786435808236826.
[48] R.A. Mulford, Analysis of strengthening mechanisms in alloys by means of thermal-activation theory, Acta Metall. 27 (1979) 1115–1124, doi:10.1016/0001-6160(79)90129-9.
[49] U.F. Kocks, A.S. Argon, M.F. Ashby, Thermodynamics and kinetics of slip, Prog. Mater. Sci. 19 (1975) 1–281, doi:10.1016/0079-6425(75)90005-5.
[50] A.H. Cottrell, R.J. Stokes, Effects of temperature on the plastic properties of aluminium crystals, Proc. R. Soc. Math. Phys. Eng. Sci. 233 (1955) 17–34, doi:10.1098/rspa.1955.0243.
[51] S.J. Basinski, Z.S. Basinski, Ch 16: plastic deformation and work hardening, in: Dislocations in Solids, edited by F.R.N. Nabarro, North-Holland Publishing Company, Amsterdam, 1979, pp. 261–362.
[52] J.G. Sevillano, Chapter 2, Flow stress and work hardening, in, Material Science and Technology - A Comprehensive Treatment, in: R.W. Cahn, P. Haasen, E.J. Kramer (Eds.), Volume 6: Plastic Deformation and Fracture of Materials, Volume Editor H. Mughrabi, Wiley-VCH Verlag GmbH & Co. KGaA, Weinheim, Germany, 2006, pp. 19–88.
[53] Z.S. Basinski, Thermally activated glide in face-centred cubic metals and its application to the theory of strain hardening, Philos. Mag. 4 (1959) 393–432, doi:10.1080/14786435908233412.
[54] R.C. Picu, R. Li, On the relationship between the Cottrell–Stokes law and the Haasen plot, Mater. Sci. Eng. A 527 (2010) 5303–5306, doi:10.1016/j.msea.2010.04.093.
[55] K. Tanoue, Cottrell-Stokes law and scaling loci of stress relaxation curves in copper single crystals, Scr. Metall. Mater. 25 (1991) 565–569, doi:10.1016/0956-716X(91)90092-F.
[56] S. Saimoto, H. Sang, A re-examination of the Cottrell-stokes relation based on precision measurements of the activation volume, Acta Metall. 31 (1983) 1873–1881, doi:10.1016/0001-6160(83)90133-5.
[57] K. Tanoue, Thermal activation analysis on the plastic deformation satisfied with the Cottrell-Stokes law, Acta Metall. Mater. 40 (1992) 1945–1950, doi:10.1016/0001-6160(83)90133-5.
[58] P.R. Thornton, T.E. Mitchell, P.B. Hirsch, The strain-rate dependence of the flow stress of copper single crystals, Philos. Mag. 7 (74) (1962) 337–358 Issue, doi:10.1080/14786436208211866.
[59] R. Zeyfang, O. Buck, A. Seeger, Thermally activated plastic deformation of high-purity copper single crystals, Phys. Status Solidi B 61 (1974) 551–561, doi:10.1002/pssb.2220610220.
[60] H. Mecking, K. Lücke, Die bestimmung des Activierungsvolumens durch wechsel des Dehnungsgeschwindigkeit insbesontere an Silberkristallen, Mater. Sci. Eng. 1 (1967) 349–359.
[61] Z.S. Basinski, Forest hardening in face centred cubic metals, Scr. Metall. 8 (1974) 1301–1307, doi:10.1016/0036-9748(74)90350-0.
[62] F.R.N. Nabarro, Work hardening of face-centered cubic single crystals, in: H.J. McQueen, J.P. Bailon, J.I. Dikson, J.J. Jonas, M.G. Akben (Eds.), Proceedings Int. Conf. on the Strength of Metals and Alloys (ICSMA 7), Strength of Metals and Alloys (ICSMA 7), 3, Pergamon Press, Oxford, 1986, pp. 1667–1700.
[63] W. Staubwasser, Uber die verfestigung von aluminium einkristallen (99,99% Al) und ihre deutung, Acta Metall. 7 (1959) 43–50, doi:10.1016/0001-6160(59)90166-X.
[64] R.W.K. Honeycombe, The Plastic Deformation of Metals, in: The Plastic Deformation of Metals, 2nd ed., Hodder Arnold, London, U.K., 1984, pp. 14–106.
[65] K. Lücke, W. Staubwasser, Uber die verfestigung von Al-einkristallen, Naturwissenschaften 41 (1954) 60 60, doi:10.1007/BF00634172.
[66] L.M. Clarebrough, M.E. Hargreaves, Work hardening of metals, Prog. Met. Phys. 8 (1959) 1–103 pp, doi:10.1016/0502-8205(59)90013-9.
[67] D. Caillard, J.L. Martin, Thermally Activated Mechanisms in Crystal Plasticity, Pergamon, Boston, Mass, 2003 Amsterdam.
[68] W. Blum, Discussion: activation volumes of plastic deformation of crystals, Scr. Mater. 146 (2018) 27–30, doi:10.1016/j.scriptamat.2017.10.029.
[69] S.W. Smith, Digital Signal Processing: A Practical Guide for Engineers and Scientists, Newnes, Boston, 2003 Amsterdam.
[70] B. Lo Piccolo, P. Spätig, T. Kruml, J.L. Martin, J. Bonneville, Characterising thermally activated dislocation mechanisms, Mater. Sci. Eng. A 309–310 (2001) 251–255, doi:10.1016/S0921-5093(00)01763-9.
[71] J.L. Martin, B. Lo Piccolo, T. Kruml, J. Bonneville, Characterization of thermally activated dislocation mechanisms using transient tests, Mater. Sci. Eng. A 322 (2002) 118–125, doi:10.1016/S0921-5093(01)01124-8.
[72] S.G.A. Verheyden, Thermal activation, intermittency and size effects in the plastic deformation of cast aluminium microwires, (2018). Ecole Polytechnique Fédérale de Lausanne, Lausanne, Switzerland, EPFL Doctoral Thesis Number 8475.
[73] G.E. Dieter, Mechanical Metallurgy, 3rd ed., McGraw-Hill, New York, 1986.
[74] H. Suzuki, S. Ikeda, S. Takeuchi, Deformation of thin copper crystals, J. Phys. Soc. Jpn. 11 (1956) 382–393, doi:10.1143/JPSJ.11.382.
[75] J. Weertman, J.R. Weertman, in: R.W. Cahn, P. Haasen (Eds.), Chapter 19: Mechanical properties, mildly temperature dependent, North-Holland Physics Publishing, Amsterdam, 1983, pp. 1259–1307.
[76] P. Haasen, Physical Metallurgy, 3rd ed., Cambridge University Press, 1984.
[77] P. Spätig, J. Bonneville, J.L. Martin, A new method for activation volume measurements: application to $Ni_3(Al,Hf)$, Mater. Sci. Eng. A 167 (1993) 73–79, doi:10.1016/0921-5093(93)90339-G.
[78] R. Bonadé, P. Spätig, The evolution of the mobile dislocation density during successive stress relaxation transients, Mater. Sci. Eng. A 483–484 (2008) 203–206, doi:10.1016/j.msea.2006.10.196.
[79] U.F. Kocks, H. Mecking, Physics and phenomenology of strain hardening: the FCC case, Prog. Mater. Sci. 48 (2003) 171–273, doi:10.1016/S0079-6425(02)00003-8.
[80] B.J. Diak, S. Saimoto, The determination of solute clusters in dilute aluminum alloys using strain rate sensitivity, Mater. Sci. Eng. A 234–236 (1997) 1019–1022, doi:10.1016/S0921-5093(97)00342-0.
[81] B.J. Diak, K.R. Upadhyaya, S. Saimoto, Characterization of thermodynamic response by materials testing, Prog. Mater. Sci. 43 (1998) 223–363, doi:10.1016/S0079-6425(98)00007-3.
[82] F. Diologent, R. Goodall, A. Mortensen, Surface oxide in replicated microcellular aluminium and its influence on the plasticity size effect, Acta Mater. 57 (2009) 286–294, doi:10.1016/j.actamat.2008.09.008.
[83] Y.-M. Chiang, D. Birnie III, W. D. Kingery, Physical Ceramics, J. Wiley & Sons, New York, 1997, page 479
[84] M. Sauzay, L.P. Kubin, Scaling laws for dislocation microstructures in monotonic and cyclic deformation of FCC metals, Prog. Mater. Sci. 56 (2011) 725–784, doi:10.1016/j.pmatsci.2011.01.006.

[85] L. Deillon, S. Verheyden, D. Ferreira Sanchez, S. Van Petegem, H. Van Swygenhoven, A. Mortensen, Laue microdiffraction characterisation of as-cast and tensile deformed Al microwires, Philos. Mag. 99 (2019) 1866–1880, doi:10.1080/14786435.2019.1605220.
[86] H.G.F. Wilsdorf, J. Schmitz, The observation and interpretation of dislocation tangles in the easy glide range of aluminum, J. Appl. Phys. 33 (1962) 1750–1754, doi:10.1063/1.1728823.
[87] H. Mughrabi, Investigations of plastically deformed copper single crystals in the stress-applied state. I. A study of the dislocation behaviour in the surface region and in the bulk, Phys. Status Solidi B 39 (1970) 317–327, doi:10.1002/pssb.19700390133.
[88] H. Mughrabi, Elektronenmikroskopische untersuchung der versetzungsanordnung verformter kupfereinkristalle im belasteten zustand, Philos. Mag. 23 (1971) 869–895 A Journal of Theoretical Experimental and Applied Physics.
[89] 6 H. Mughrabi, A.S. Argon, Description of the dislocation structure after unidirectional deformation at low temperatures, in: in: Constitutive Equations in Plasticity, A.S. Argon Editor,, The MIT Press, Cambridge Mass., 1975, pp. 199–250.
[90] U. Essmann, M. Rapp, Slip in copper crystals following weak neutron bombardment, Acta Metall. 21 (1973) 1305–1317, doi:10.1016/0001-6160(73)90172-7.
[91] A.S. Argon, G. East, A statistical theory for easy glide, Transactions Japan Institute for Metals (Trans. JIM) 9 (Supplement: Proc. of the Int. Conf. on the Strength of Metals and Alloys) (1968) 756–767.
[92] A.S Argon, A statistical theory for easy glide II, Physics of Strength and Plasticity, A.S. Argon Editor, MIT Press, Cambridge Mass, 1969, pp. 217–245.
[93] P. Veyssière, H. Wang, D.S. Xu, Y.L. Chiu, Local dislocation reactions, self-organization and hardening in single slip, IOP Conf. Ser. Mater. Sci. Eng. 3 (2009) 012018, doi:10.1088/1757-899X/3/1/012018.
[94] P. Veyssière, Y.L. Chiu, M. Niewczas, Dislocation micromechanisms under single slip conditions, Z. Metallkd. 97 (2006) 189–199, doi:10.3139/146.101242.
[95] H. Mughrabi, Some consequences of surface and size effects in plastically deformed copper single crystals, Phys. Status Solidi B 44 (1971) 391–402, doi:10.1002/pssb.2220440140.
[96] F.R.N. Nabarro, in: Theory of Crystal Dislocations, Dover Publications, New York, 1967, pp. 267–302.
[97] J.T. Fourie, The flow stress gradient between the surface and the centre of deformed copper single crystals, Philos. Mag. 17 (148) (1968) 735–756.
[98] F.R.N. Nabarro, in: R.M. Latanision, J.T. Fourie (Eds.), Surface effects in crystal plasticity – overview from the crystal plasticity standpoint, Surface Effects in Crystal Plasticity, Nato Advanced Study Institute Series, Series E – Applied Science No. 17, Noordhoff, Leiden, 1977, pp. 49–125.